Nanostructuring of laser textured surface to achieve superhydrophobicity on engineering metal surface

Cite as: J. Laser Appl. **31**, 022515 (2019); doi: 10.2351/1.5096148 Submitted: 14 March 2019 · Accepted: 14 March 2019 · Published Online: 19 April 2019







Avik Samanta, 1,a) (D) Qinghua Wang, 1,a) (D) Scott K. Shaw, 2 and Hongtao Ding 1,b)

AFFILIATIONS

- ¹Department of Mechanical Engineering, University of Iowa, Iowa City, Iowa 52242
- ²Department of Chemistry, University of Iowa, Iowa City, Iowa 52242

Note: This paper is part of the Special Collection: Proceedings of the International Congress of Applications of Lasers & Electro-Optics (ICALEO® 2018).

- a)Contributions: Avik Samanta and Qinghua Wang contributed equally to this paper.
- ^{b)}Author to whom correspondence should be addressed; electronic mail: hongtao-ding@uiowa.edu

ABSTRACT

Superhydrophobic metal alloy surfaces are increasingly employed in aerospace and naval applications for anti-icing, drag reduction, self-cleaning, and high-efficiency light absorption capabilities. Emerging laser-based surface texturing methods demonstrate significant potential for manufacturing these surfaces, with the advantages of high processing precision and flexibility. In this research, superhydrophobicity is achieved on engineering metal surfaces using a novel nanosecond Laser-based High-throughput Surface Nanostructuring process. First, a high-energy nanosecond pulse laser scans the metal surface submerged in water using a large spatial increment and a fast processing speed. After that, the laser-textured surface is further treated by immersion in a chlorosilane reagent for a specific period of time. As a result of these two processes, micro- and nano-scale surface features are generated on the metal surface. These features are measured on AISI 4130 steel workpieces through scanning electron microscopy. The surface chemistry is characterized by x-ray photoelectron spectroscopy and correlated with processing conditions. The features are also compared after completion of each process step to understand their individual and cumulative effect on the textured surface. It is found that utilizing a high laser power intensity during the laser texturing process phase will significantly enhance surface nanostructuring effects after the chlorosilane treatment, resulting in feature size decrease and increase in feature density.

Key words: surface texturing, nanosecond laser, nanostructuring, superhydrophobicity, chlorosilane

© 2019 Laser Institute of America. https://doi.org/10.2351/1.5096148

I. INTRODUCTION

Recently, functional engineering surface has attracted the attention of researchers due to its great potential in multifunctional applications. One of the prime examples of multifunctional surfaces is superhydrophobic metal alloy surfaces that are increasingly being employed in aerospace and naval applications. Superhydrophobic phenomenon was first discovered on plant leaves, insect legs, and wings, while people have spent decades on the biomimetic trail. Superhydrophobic surface has some excellent surface properties for anti-icing, are duction, self-cleaning, anti-biofouling, and high-efficiency light absorption capabilities.

anticorrosion, anti-biofouling, and anti-icing properties of superhydrophobic metal surfaces are utilized for marine surfaces to extend their lives, especially in extreme cold arctic regions.²³ Modern aerospace industry deploys the anti-icing, self-cleaning, and solar light absorption capabilities of hydrophobic surfaces for future solar aircraft.²⁴ Three main techniques are widely used to prepare superhydrophobic multifunctional surface: (a) top-down approach, which removes material from bulk workpiece to create nanoscale structures using energy sources, chemical, and electrochemical processes;^{14–16,22} (b) bottom-up approach, which builds up nanoscale features though nanomanufacturing from atomic and molecular-scale components;^{25,26} and (c) a combination of top-down and

bottom-up approach.²⁷ The top-down approach is a comparatively faster and economically feasible process for industrial applications.

Emerging laser-based surface texturing methods demonstrate significant potential for manufacturing functional surfaces, with the additional advantages of maintaining high precision and process flexibility. Existing laser-based surface texturing methods often employ ultrashort pulse lasers to generate microscale patterns or periodic nanoscale features on metallic materials. 14,16,20,21,28 Considerable investigation has been afforded two primary ultrashort laser-based surface texturing methods: (1) laser-induced periodic surface structure (LIPSS) consisting of laser-induced surface ripples with periodicity equal to or smaller than the wavelength of the laser radiation; ^{21,29,30} and (2) laser surface inscribing to achieve hierarchical structures consisting of ordered microstructures (e.g., parallel microgrooves). 15,22,36,40 To create these surface structures, both methods scan metal surfaces at a very fine spatial resolution for which a long processing time for a given unit of area is required. Extensive research in the past decade has shown that a metal surface textured using ultrashort laser scanning is inherently hydrophilic.3

In order to achieve a hydrophilicity-to-superhydrophobicity transition, the chemical composition of the laser-textured surface must be altered to reduce surface energy. Various post-laser process methods have been applied to ultrashort laser pretextured metal surfaces, including a chemical surface treatment process^{33–35} or a long-term storage period (characteristically in air for several weeks). 14,16,32,33,38,39,45 Steele *et al.* 33 fabricated LIPSS consisting of cone-like microstructure on pure titanium substrates using a femtosecond pulse laser with subsequent application of fluoropolymer coating on top of the laser-textured surface. These results showed that the laser-textured surface with fluoropolymer coating exhibited superhydrophobicity with a contact angle of 165°. Vorobyev and Guo, 15 experimenting with platinum, titanium, and brass, used a femtosecond pulse laser to create omnidirectional microgrooves consisting of hierarchical microstructures. Specimens reportedly achieved hydrophilicity immediately after femtosecond laser surface structuring but required long exposure in air to achieve superhydrophobicity. The transition occurred predominantly due to chemical interaction between the surface and the ambient CO2, resulting in an accumulation of carbon and carbon compounds on the lasertreated surface. Martínez-Calderon et al.36 investigated the wetting behavior for AISI 304 stainless steel alloy for different types of surface structures using a femtosecond pulse laser, including omnidirectional trenches, cross-hatch trenches, omnidirectional trenches covered by LIPSS, and cross-hatch trenches covered by LIPSS. An additional laser texturing step was required to create LIPSS over the microstructured specimens. All specimens subject to femtosecond laser texturing were hydrophilic, with an initial contact angle less than 30° directly after laser treatment. After storing in air for more than 120 h, these surfaces became hydrophobic and superhydrophobic for microstructured (omnidirectional or cross-hatch trenches) specimens and hierarchical structured (omnidirectional or cross-hatch trenches covered with LIPSS) specimens, respectively.

It should be emphasized that these state-of-the-art surface treatment methods rely on a laser texturing phase to generate surface micro-/nanoscale features. Surface nanostructuring effects have never been observed in any of these existing postlaser processes. It is generally believed that silane-based surface modification treatments provide only a surface coating effect, for which etching in metal alloys would not occur during postprocessing subsequent to ultrashort laser texturing. In contrast to this conventional understanding of surface silanization, this study shows that chemical surface treatment induces simultaneous silanization effects and significant chemical etching for metal surfaces prepared using laser texturing.

II. EXPERIMENTAL PROCEDURE

A novel nanosecond Laser-based High-throughput Surface Nanostructuring (nHSN) process is developed for engineering metal alloys to achieve superhydrophobic surfaces. This novel process consists of two steps: (1) water-confined nanosecond laser texturing, during which a high-energy nanosecond pulse laser scans the material surface contained under water using a large spatial increment and a fast processing speed, (2) chemical immersion treatment, during which the laser-textured surface is further chemically treated.

A. Water-confined nanosecond laser texturing

The experimental setup for the water-confined nanosecond laser texturing tests uses a Q-Switched Nd:YAG nanosecond laser (Spectra-Physics Quanta-Ray Lab-150, wavelength 1064 nm) with a high energy per pulse on the order of several hundreds of mJ/pulse. During the laser texturing process, the laser repetition rate is 10 pulses per second with a laser pulse duration of 6–8 ns. A galvanometer laser scanner (SCANLAB intelliSCAN* 20) furnished with an f-theta objective with a focal length of 255 mm directs the laser to texture the top surface of the specimen. The specimen is submerged in deionized water, which confines the laser pulse-induced plasma and enhances the texturing effect.

Figure 1(a) shows the schematic representation of the waterconfined nanosecond laser texturing system. The workpiece is kept under deionized water confinement (around 8 mm depth from the water surface) in a tank, which is positioned using computercontrolled stages. Figure 1(b) shows the typical laser scanning path used during the experiments. The laser scan head scans the top surface of the work material in a zig-zag pattern as shown in Fig. 1(b). The X-spacing (or pitch) defines the distance between two sequential laser scan lines and is pre-set through computer control. The Laser Scan Line Density, as determined by Eq. (1), defines how many laser scan lines are required to scan a 1-in. width area. The Y-spacing between two sequential laser shots along the scanning direction is determined by the Laser Repetition Rate and pre-set Laser Scanning Speed as in Eq. (2). The Overlap Ratio is set by the ratio of Overlap Area to the Laser Spot Area as in Eq. (3). For all the experimental conditions in this study, the same value was applied for both X-spacing and Y-spacing, which guarantees the same Overlap Ratio of 50% in both directions. The Laser Spot Area can be adjusted by moving the Z stage away from the focal plane

Laser Scan Line Density (lines/in.) =
$$\frac{1 \text{ in.}}{X\text{-spacing}}$$
, (1)

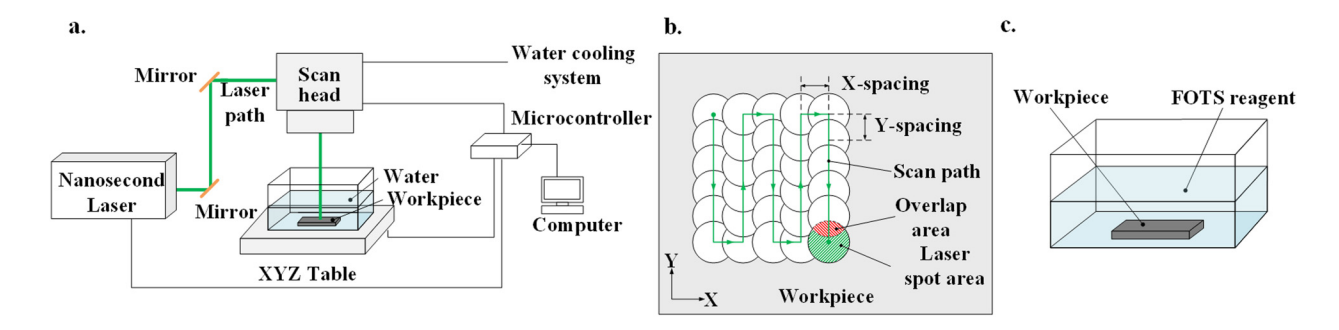


FIG. 1. Schematic representation of the process: (a) experimental setup of water-confined nanosecond laser texturing; (b) laser scanning path; (c) experimental setup of chemical immersion treatment.

$$Y\text{-spacing} = \frac{\text{Laser Scanning Speed}}{\text{Laser Repetition Rate}},$$
 (2)

Overlap Ratio =
$$\frac{\text{Overlap Area}}{\text{Laser Spot Area}} \times 100\%$$
. (3)

The combination of laser scan head and computer-controlled stages allows having a wide range of laser scanning area during the process. Both laser and scan head are controlled by a microcontroller for scanning along a predesigned path. The scan head is also connected to a water cooling system to avoid any undesirable heating of the scan head during the process.

B. Chemical immersion treatment

After the laser texturing, the workpieces were immersed in an ethanol solution with 1.5% volume percentage cholosilane reagent $[CF_3(CF_2)_5(CH_2)_2SiCl_3]$, also known as FOTS at room temperature for \sim 3 h as shown in Fig. 1(c). Workpieces were then cleaned with deionized water and dried using compressed air. Finally, it was kept at 80 °C in a vacuum oven for 1 h to dry it out completely.

C. Measurements and characterization

Water contact angle (WCA) for the treated specimen surface was measured during the wettability test using a contact angle goniometer (Rame-Hart model 100) coupled with a high-resolution CMOS camera (6–60× magnification, Thor Laboratories). For each WCA measurement, about $4\,\mu l$ volume of water was dropped to form a still water droplet on the specimen surface, and its optical shadowgraph was obtained using the CMOS camera. The optical shadowgraph was quantitatively analyzed using $_{\rm IMAGEJ}$ software to determine the WCA for each measurement. Multiple WCA measurements were performed at various locations inside each specimen surface, and the average value of measurement results was obtained.

The surface morphology of the superhydrophobic surface was analyzed using a scanning electron microscope (Hitachi S-4800). The scanning electron microscopy (SEM) images were taken at 1.8–2.0 kV acceleration voltages. Additionally, x-ray photoelectron

spectroscopy (XPS) analysis was carried out for the surface chemistry using Kratos Axis Ultra high-performance XPS system. To investigate the chemical composition at a certain depth, the surface was etched by 100 nm by ion-gun etching cycles between two adjacent XPS measurements. Full survey spectra and high-resolution elemental spectra were acquired for surface composition analysis and chemical state identification, respectively.

III. RESULTS AND DISCUSSIONS

A. Water contact angle

The wettability of the specimen surface produced by developed process was experimentally evaluated through water wetting tests. The definition of surface wettability can be described as the tendency of a liquid to spread on or adhere to a solid surface without the formation of droplets. When the liquid is water, it completely wets the hydrophilic surface without the formation of droplets while water droplets will form on hydrophobic surfaces. WCA is one of the quantitative methods to define how water interacts with a solid surface without absorbing the water, dissolving in the water or reacting with the water. It is defined as the angle, conventionally measured through the water droplet, where water–vapor interface meets a solid surface and can be used to quantify the wettability of a solid surface.

As illustrated in Fig. 2(a), the surface wettability to water can be categorized into four categories: hydrophobic, hydrophilic, superhydrophobic, and superhydrophilic. If WCA is less than 30°, the surface is designated superhydrophilic, and the water completely spreads over the surface. If the WCA is in between 30° and 90°, the surface is categorized as hydrophilic. On a hydrophobic surface, water forms distinct droplets. As the hydrophobicity increases, the contact angle of the droplets with the surface increases. Surfaces with WCA in between 90° and 150° are designated as hydrophobic. When WCA is greater than 150°, the surface is generally regarded as superhydrophobic.

Figure 2(b) illustrates the sprayed water droplets formed on the AISI 4130 steel specimen surface treated by the process developed in this study. It can be noted that completely spherical water droplets form on the processed surface, demonstrating the superhydrophobicity. Figure 3 shows the water contact angle measurement

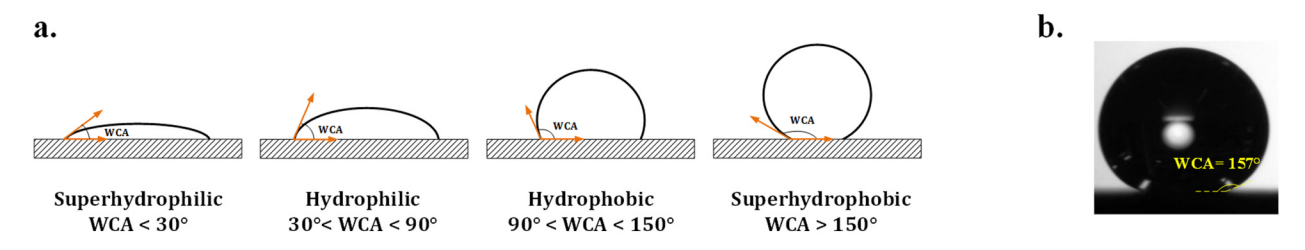


FIG. 2. (a) Schematic representation of four exemplary scenarios of WCA. (b) Measured WCA in the superhydrophobic AISI 4130 steel surface.

results for AISI 4130 steel specimens produced by the laser surface texturing process using various laser power intensities ranging from 0.1 to 18.2 GW/cm². The uncertainty was typically around ±2° for each test. The measurement for 0 GW/cm² was performed on the specimens produced by the chemical immersion treatment alone without any prior laser texturing, and their results show a WCA of 96.9°. The specimens treated by low laser power intensities from 0.1 GW/cm² during the laser texturing step showed improved hydrophobicity with increased WCA up to 111.1°. These tests also indicated that a higher laser power intensity helped increase the WCA during the process. Further increase in laser power intensity during the texturing process improved the WCA in the superhydrophobic range. All the specimens treated by laser power intensities from 0.2 to 18.2 GW/cm² achieved superhydrophobicity with WCA greater than 150°. Varying laser power intensity did not significantly alter the WCA for these superhydrophobic AISI 4130 steel specimens. These results indicated that a wide process window existed to produce consistent superhydrophobic AISI 4130 steel surfaces, as long as the laser power intensity was equal or greater than 0.2 GW/cm².

B. Surface nanostructure

The surface microstructures were analyzed for various specimens directly after the laser texturing and after the chemical

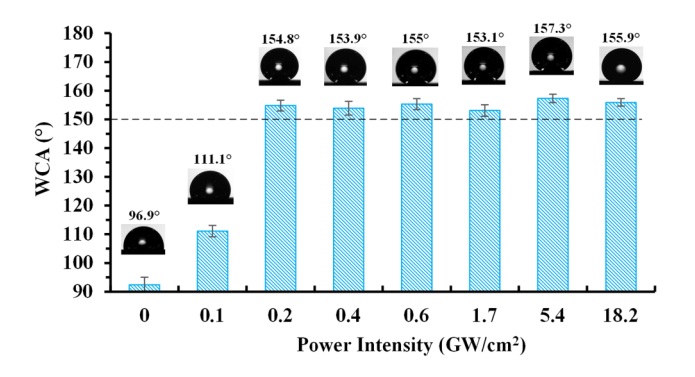


FIG. 3. Contact angle measurement results for AISI 4130 steel specimens produced by the nHSN process at various laser power intensities ranging from 0 (indicating no laser texturing and only chemical immersion treatment) to 18.2 GW/cm².

treatment as illustrated in Fig. 4. In this study, the specimens were processed by the same laser power intensity of 0.6 GW/cm². Therefore, the only difference between the two samples was that one went through the chemical immersion treatment while the other did not. Micrographs at different magnifications ranging from 100× to 20 000× are shown in Fig. 4. In comparison, at 100× magnification with a view area of about 1 mm², both the specimens show an isotropic texture. There is no significant difference between the surfaces without any obvious lay pattern as shown in Figs. 4(a) and 4(d). At 5000× magnification, significantly different surface microstructures can be observed as illustrated in Figs. 4(b) and 4(e). Numerous tiny pores and thermal cracks and microscale ripples can be observed immediately after laser texturing, whereas spherical micro-/nanostructures were homogenously distributed over the other specimen that underwent chemical immersion treatment after laser texturing. The microscale ripples were induced from the nanosecond laser-steel interaction under water confinement on the specimen after laser texturing, which were not observed after chemical immersion treatment. This indicated the chemical immersion treatment significantly modified the surface morphology. At 20 000× magnification with a view area of about $30 \,\mu\text{m}^2$, the pores and thermal cracks were more clearly observed in Fig. 4(c) on the specimen with only laser texturing, whereas nanoscale spherical protrusions, rods, cones, platelets, and pores with size of few hundreds of nanometers are observed on the sample which went through chemical immersion treatment after laser texturing [Fig. 4(f)].

C. Chemistry analysis

The elemental composition of the treated surface was investigated using the XPS survey of the surface and at a 100 nm depth as illustrated in Fig. 5. It can be observed that immediately after waterconfined laser texturing, elements such as oxygen, carbon, and iron were detected on the laser-textured surface and their corresponding intensities were reduced as the etched depth increased to 100 nm. The iron and carbon came from the composition of AISI 4130 steel and oxygen came from the oxidation/hydroxylation happened during water-confined laser texturing [Fig. 5(a)]. For the sample which went through both water confined laser texturing and subsequent chemical immersion treatment, significantly different XPS spectra were observed. Two additional peaks in fluorine and silicon along with oxygen, carbon, and iron were observed in the survey at the surface [Fig. 5(b)]. Those two peaks were completely gone at the etched

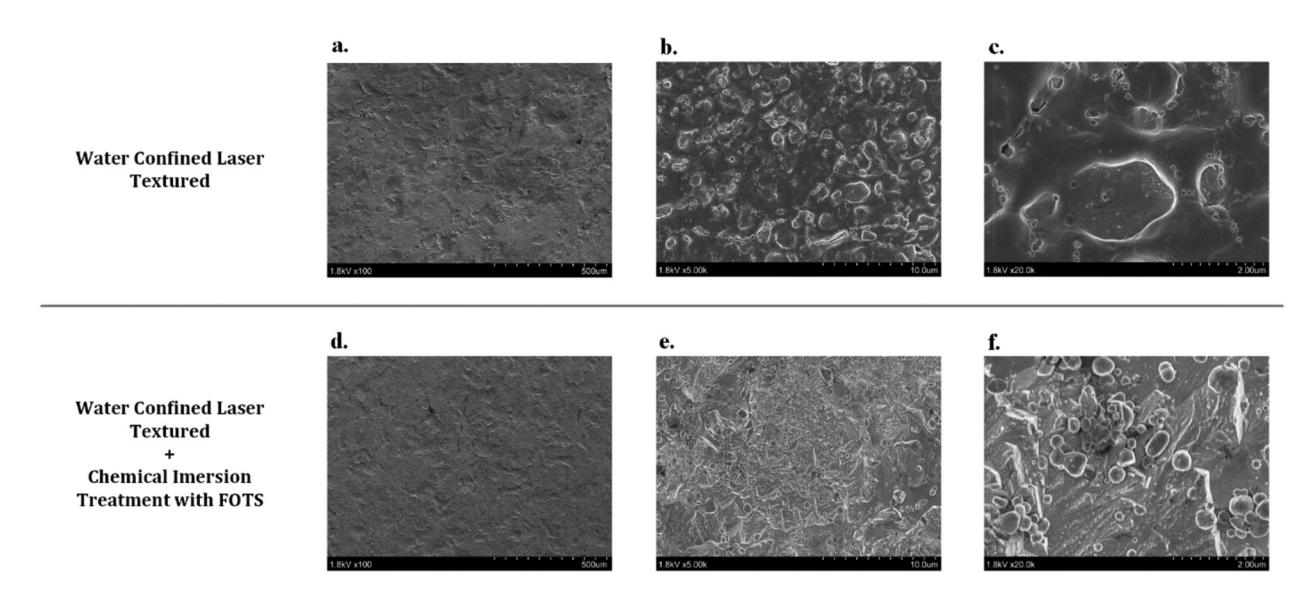


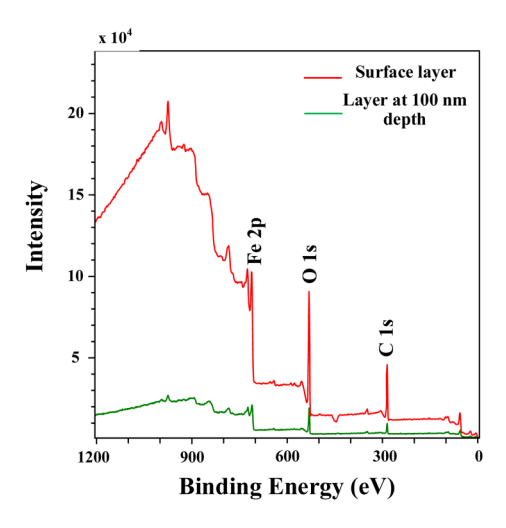
FIG. 4. SEM micrographs of two AISI 4130 steel specimens. At top: specimen processed water-confined laser texturing with laser power intensity of 0.6 GW/cm² at various magnifications: (a) 100×, (b) 5000×, and (c) 20 000×. At bottom: specimen processed with chemical immersion treatment after water-confined laser texturing with laser power intensity of 0.6 GW/cm² at various magnifications: (d) 100×, (e) 5000×, and (f) 20 000×.

depth of 100 nm. The source of fluorine and silicon belonged to FOTS cholosilane reagent $[CF_3(CF_2)_5(CH_2)_2SiCl_3]$. $-CF_2$ - and $-CF_3$ groups present on the cholosilane structure were attached to the processed surface leading to surface fluorination. $-CF_2$ - and $-CF_3$ groups are known to be low binding energy groups, so with their attachment to the surface, surface energy was reduced that contributed to the superhydrophobicity. Surprisingly, no chlorine signal was observed in the XPS survey though there is chlorine in the FOTS reagent. It is hypothesized that the chlorine elements in FOTS

cholosilane reagent reacted with metal oxide and dissolved in the chemical solution.

After the chemical immersion treatment, postprocess liquid solution was chemically tested to find out the etched away metal elements in the solution. Sodium hydroxide (NaOH) and deionized water were added to the solution. After sometime, reddishbrown precipitates were formed as shown in Fig. 6. From the color of the precipitates, they are believed to be ferric hydroxide [Fe(OH)₃], which is insoluble in water. This definitely proved

a. After laser texturing



b. After laser texturing + chemical immersion treatment

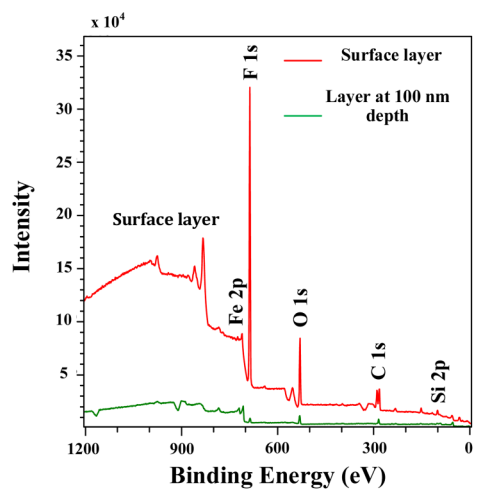


FIG. 5. XPS survey of the surface layer and at 100 nm depth for (a) specimen underwent water-confined laser texturing and (b) specimen underwent both water-confined laser texturing and subsequent chemical immersion treatment with FOTS cholosilane reagent.

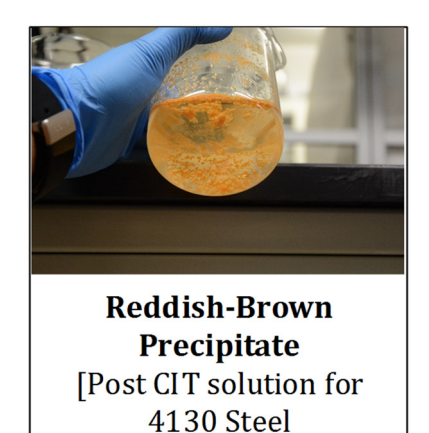


FIG. 6. Chemical analysis to show etching effect that brought Fe elements to the solution

+ NaOH + DI Water]

that etching happened due to chlorine during the chemical immersion treatment that brought Fe elements from substrate to the solution. This finding would contribute to the nanostructure formation as discussed in Sec. II B.

IV. CONCLUSIONS

A novel water-confined nanosecond laser texturing method coupled with chemical immersion treatment was successfully developed for producing superhydrophobic AISI 4130 steel surface. The process is completely different from the state-of-the-art laserinduced periodic surface structures produced from existing ultrashort laser-based surface texturing methods. Wide range of laser power intensities ranging from 0.2 to 18.2 GW/cm² were used to produce stable superhydrophobic surface with WCA consistently greater than 150°. Nanoscale surface protrusions, rods, cones, platelets, and pores with size of few hundreds of nanometers were observed in microstructure analysis that contributed for superhydrophobicity. Surface chemical analysis was also performed using XPS. It showed the presence of -CF₂- and -CF₃ groups on the surface, confirming the occurrence of surface fluorination in specimens during chemical immersion treatment. Low binding energy -CF2and -CF3 groups reduced surface energy and led to an enhancement of surface hydrophobicity.

ACKNOWLEDGMENT

The authors gratefully acknowledge the financial support by the National Science Foundation (NSF) under Grant No. CMMI-1762353.

REFERENCES

¹T. Darmanin and F. Guittard, "Superhydrophobic and superoleophobic properties in nature," Mater. Today 18, 273–285 (2015).

- ²X. Gao and L. Jiang, "Water-repellent legs of water striders," Nature 432, 36 (2004).
- ³T. Wagner, C. Neinhuis, and W. Barthlott, "Wettability and contaminability of insect wings as a function of their surface sculptures," Acta Zool. 77, 213–225 (1996).
- ⁴E. A. Bogoslov, M. P. Danilaev, S. A. Mikhailov, and Y. E. Pol'skii, "Energy efficiency of an integral anti-ice system based on fluoroplastic films," J. Eng. Phys. Thermophys. **89**, 815–820 (2016).
- ⁵L. Cao, A. K. Jones, V. K. Sikka, J. Wu, and D. Gao, "Anti-Icing superhydrophobic coatings," Langmuir 25, 12444–12448 (2009).
- ⁶M. Ruan, W. Li, B. Wang, B. Deng, F. Ma, and Z. Yu, "Preparation and antiicing behavior of superhydrophobic surfaces on aluminum alloy substrates," Langmuir 29, 8482–8491 (2013).
- ⁷L. B. Boinovich, A. M. Emelyanenko, K. A. Emelyanenko, and K. I. Maslakov, "Anti-icing properties of a superhydrophobic surface in a salt environment: an unexpected increase in freezing delay times for weak brine droplets," Phys. Chem. Chem. Phys. 18, 3131–3136 (2016).
- ⁸R. Truesdell, A. Mammoli, P. Vorobieff, F. Van Swol, and C. J. Brinker, "Drag reduction on a patterned superhydrophobic surface," Phys. Rev. Lett. **97**, 1–4 (2006).
- ⁹J. W. Gose, K. Golovin, A. Tuteja, S. L. Ceccio, and M. Perlin, "Experimental investigation of turbulent skin-friction drag reduction using superhydrophobic surfaces," in 31st Symposium on Naval Hydrodynamics, Monterey, California, 11–16 September 2016, pp. 11–16.
- ¹⁰T. Min and J. Kim, "Effects of hydrophobic surface on skin-friction drag," Phys. Fluids 16, 1–5 (2004).
- ¹¹X. Pu, G. Li, and H. Huang, "Preparation, anti-biofouling and drag-reduction properties of a biomimetic shark skin surface," Biol. Open 5, 389LP-396LP (2016).
- ¹²L. R. de Lara, R. Jagdheesh, and J. L. Ocana, "Corrosion resistance of laser patterned ultrahydrophobic aluminium surface," Mater. Lett. **184**, 100–103 (2016).
- ¹³Z. Lu, P. Wang, and D. Zhang, "Super-hydrophobic film fabricated on aluminium surface as a barrier to atmospheric corrosion in a marine environment," Corros. Sci. 91, 287–296 (2015).
- ¹⁴R. Jagdheesh, M. Diaz, and J. L. Ocaña, "Bio inspired self-cleaning ultrahydro-phobic aluminium surface by laser processing," RSC Adv. 6, 72933–72941 (2016).
- ¹⁵A. Y. Vorobyev and C. Guo, "Multifunctional surfaces produced by femtosecond laser pulses," J. Appl. Phys. 117, 033103 (2015).
- ¹⁶D. V. Ta, A. Dunn, T. J. Wasley, R. W. Kay, J. Stringer, P. J. Smith, C. Connaughton, and J. D. Shephard, "Nanosecond laser textured superhydrophobic metallic surfaces and their chemical sensing applications," Appl. Surf. Sci. 357, 248–254 (2015).
- 17K. Sun, H. Yang, W. Xue, A. He, D. Zhu, W. Liu, K. Adeyemi, and Y. Cao, "Anti-biofouling superhydrophobic surface fabricated by picosecond laser texturing of stainless steel," Appl. Surf. Sci. 436, 263–267 (2018).
- ¹⁸M. Ferrari, A. Benedetti, E. Santini, F. Ravera, L. Liggieri, E. Guzman, and F. Cirisano, "Biofouling control by superhydrophobic surfaces in shallow euphotic seawater," Colloids Surf. A Physicochem. Eng. Asp. 480, 369–375 (2015).
- ¹⁹Z. Ou, M. Huang, and F. Zhao, "The fluence threshold of femtosecond laser blackening of metals: The effect of laser-induced ripples," Opt. Laser Technol. 79, 79–87 (2016).
- ²⁰M. Huang, F. Zhao, Y. Cheng, N. Xu, and Z. Xu, "The morphological and optical characteristics of micro/nanostructures on GaAs, Si, and brass," Opt. Express 18(S4), A600–A619 (2010).
- 21B. K. Nayak and M. C. Gupta, "Self-organized micro/nano structures in metal surfaces by ultrafast laser irradiation," Opt. Lasers Eng. 48, 940–949 (2010).
- ²²M. V. Rukosuyev, J. Lee, S. J. Cho, G. Lim, and M. B. G. Jun, "One-step fabrication of superhydrophobic hierarchical structures by femtosecond laser ablation," Appl. Surf. Sci. 313, 411–417 (2014).
- ²³N. P. Gule, N. M. Begum, and B. Klumperman, "Advances in biofouling mitigation: A review," Crit. Rev. Environ. Sci. Technol. 46, 535–555 (2016).

- ²⁴E. Baharozu, G. Soykan, and M. B. Ozerdem, "Future aircraft concept in terms of energy efficiency and environmental factors," Energy 140, 1368–1377 (2017).
- ²⁵P. M. Hansson, A. Swerin, J. Schoelkopf, P. A. C. Gane, and E. Thormann, "Influence of surface topography on the interactions between nanostructured hydrophobic surfaces," Langmuir 28, 8026–8034 (2012).
- ²⁶E. Bormashenko, T. Stein, G. Whyman, Y. Bormashenko, and R. Pogreb, "Wetting properties of the multiscaled nanostructured polymer and metallic superhydrophobic surfaces," <u>Langmuir</u> 22, 9982–9985 (2006).
- ²⁷M. H. Kwon, H. S. Shin, and C. N. Chu, "Fabrication of a super-hydrophobic surface on metal using laser ablation and electrodeposition," Appl. Surf. Sci. 288, 222–228 (2014).
- ²⁸T. Chen, H. Liu, H. Yang, W. Yan, W. Zhu, and H. Liu, "Biomimetic fabrication of robust self-assembly superhydrophobic surfaces with corrosion resistance properties on stainless steel substrate," RSC Adv. 6, 43937–43949 (2016).
 ²⁹D. M. Chun, C. V. Ngo, and K. M. Lee, "Fast fabrication of superhydrophobic
- ²⁹D. M. Chun, C. V. Ngo, and K. M. Lee, "Fast fabrication of superhydrophobic metallic surface using nanosecond laser texturing and low-temperature annealing," CIRP Ann. Manuf. Technol. **65**, 519–522 (2016).
- ³⁰J. Long, P. Fan, M. Zhong, H. Zhang, Y. Xie, and C. Lin, "Superhydrophobic and colorful copper surfaces fabricated by picosecond laser induced periodic nanostructures," Appl. Surf. Sci. 311, 461–467 (2014).
- ³¹M. K. Tang, X. J. Huang, Z. Guo, J. G. Yu, X. W. Li, and Q. X. Zhang, "Fabrication of robust and stable superhydrophobic surface by a convenient, low-cost and efficient laser marking approach," Colloids Surf. A Physicochem. Eng. Asp. 484, 449–456 (2015).
- ³²V. D. Ta, A. Dunn, T. J. Wasley, J. Li, R. W. Kay, J. Stringer, P. J. Smith, E. Esenturk, C. Connaughton, and J. D. Shephard, "Laser textured superhydrophobic surfaces and their applications for homogeneous spot deposition," Appl. Surf. Sci. 365, 153–159 (2016).
- ³³A. Steele, B. K. Nayak, A. Davis, M. C. Gupta, E. Loth, S. Adam, K. N. Barada, D. Alexander, C. G. Mool, and L. Eric, "Linear abrasion of a titanium superhydrophobic surface prepared by ultrafast laser microtexturing," J. Micromech. Microeng. 23, 115012 (2013).
- ³⁴B. Wu, M. Zhou, J. Li, X. Ye, G. Li, and L. Cai, "Superhydrophobic surfaces fabricated by microstructuring of stainless steel using a femtosecond laser," Appl. Surf. Sci. 256, 61–66 (2009).

- ³⁵B. Li, H. Li, L. Huang, N. Ren, and X. Kong, "Femtosecond pulsed laser textured titanium surfaces with stable superhydrophilicity and superhydrophobicity," Appl. Surf. Sci. 389, 585–593 (2016).
- 36M. Martínez-Calderon, A. Rodríguez, A. Dias-Ponte, M. C. Morant-Miñana, M. Gómez-Aranzadi, and S. M. Olaizola, "Femtosecond laser fabrication of highly hydrophobic stainless steel surface with hierarchical structures fabricated by combining ordered microstructures and LIPSS," Appl. Surf. Sci. 374, 81–89 (2016).
- ³⁷A. Cunha, A. P. Serro, V. Oliveira, A. Almeida, R. Vilar, and M. C. Durrieu, "Wetting behaviour of femtosecond laser textured Ti-6Al-4V surfaces," Appl. Surf. Sci. **265**, 688–696 (2013).
- ³⁸P. Bizi-Bandoki, S. Valette, E. Audouard, and S. Benayoun, "Time dependency of the hydrophilicity and hydrophobicity of metallic alloys subjected to femtosecond laser irradiations," Appl. Surf. Sci. 273, 399–407 (2013).
- ³⁹A. M. Kietzig, S. G. Hatzikiriakos, and P. Englezos, "Patterned superhydrophobic metallic surfaces," Langmuir 25, 4821–4827 (2009).
- ⁴⁰S. Sarbada and Y. C. Shin, "Superhydrophobic contoured surfaces created on metal and polymer using a femtosecond laser," Appl. Surf. Sci. 405, 465–475 (2017).
- ⁴¹R. Jagdheesh, B. Pathiraj, E. Karatay, G. R. B. E. Römer, and A. J. Huis In'T Veld, "Laser-induced nanoscale superhydrophobic structures on metal surfaces," Langmuir 27, 8464–8469 (2011).
- ⁴²J. Long, M. Zhong, H. Zhang, and P. Fan, "Superhydrophilicity to superhydrophobicity transition of picosecond laser microstructured aluminum in ambient air," J. Colloid Interface Sci. 441, 1–9 (2015).
- ⁴³B. Liu, W. Wang, G. Jiang, X. Mei, Z. Wang, K. Wang, and J. Cui, "Study on hierarchical structured PDMS for surface super-hydrophobicity using imprinting with ultrafast laser structured models," Appl. Surf. Sci. 364, 528–538 (2016).
- ⁴⁴Y. Yang, J. Yang, C. Liang, and H. Wang, "Ultra-broadband enhanced absorption of metal surfaces structured by femtosecond laser pulses," Opt. Express 16, 11259–11265 (2008).
- ⁴⁵M. Tang, V. Shim, Z. Y. Pan, Y. S. Choo, and M. H. Hong, "Laser ablation of metal substrates for super-hydrophobic effect," J. Laser Micro/Nanoeng. **6**, 6–9 (2011).